Available online www.ejaet.com

European Journal of Advances in Engineering and Technology, 2015, 2(1): 21-29

Research Article ISSN: 2394 - 658X

A New Machine Learning Algorithm for Breast and Pectoral Muscle Segmentation

Huda Al-Ghaib, Yi Wang and Reza Adhami

Department of Electrical and Computer Engineering, The University of Alabama in Huntsville, Alabama, USA
hag0002@uah.edu

ABSTRACT

Automatic mammogram registration provides information about gradual changes in temporal mammograms. Segmentation of landmarks such as the breast, breast skin line, and pectoral muscle are required for this process. This paper presents a new machine learning algorithm, known as margin setting algorithm (MSA), to segment the breast and pectoral muscle. MSA creates multiple prototypes to enclose patterns belonging to different classes. In this research, we applied MSA to segment the breast and pectoral muscle. The performance of our algorithm is compared with four different algorithms; neural network (NN), and three thresholding algorithms; ant colony optimization (ACO), global, and Otsu. These algorithms were tested on 554 mammograms from 125 patients. Subjective evaluation, by four researchers in the area of pattern recognition, was used to compare the outcomes. MSA outperformed NN algorithm in 84.21% of the mammograms. Also, MSA outperformed the other three algorithms in 98.12% of the mammograms.

Key words: Margin setting algorithm, machine learning, hyperspheres, thresholding and mammogram registration

---

INTRODUCTION

Image segmentation is the process of extracting meaningful information from an image for a specific task or application. It partitions the image into different portions or segments using different techniques [1-3]. Segmentation algorithms can vary from a simple algorithm that uses the range of the image intensities to compute a threshold value to a complex algorithm that utilizes various image processing tools and algorithms. Usually, the image type and the information needed to be extracted determine the segmentation method. Segmentation algorithms can be subdivided into three categories; thresholding, boundary detection, and region merging. In the thresholding category, a threshold value is computed to separate an object of interest from the background. Image histogram can be used for this purpose to determine the value that subdivides the image into two classes, i.e., object and background classes. These two classes contain all the pixel values that are below and above a threshold value. This algorithm is known as global thresholding with one threshold value applied to the entire image. When the threshold value varies in different image regions it is known as local or variable thresholding [1]. Thresholding provides good results when the object is easily separable from the background. Boundary detection segmentation algorithms attempt to detect an object using its boundary. This can be done by computing the local maximum gradient or the zero-crossing of the second derivative. Algorithms such as Laplacian or Canny can be used for this category. In the third category, adjacent similar intensity values are combined together to merge similar regions and detect objects. Watershed and morphological algorithms can be used for this purpose [1].

Segmentation is widely used in many real time applications. This paper explores the applications of segmentation in mammography. Mammogram segmentation is used for lesion detection and landmark detection for the purpose of mammogram registration. Also, segmentation can be used to remove or discard unnecessary information such as background, labels, or even some breast tissues. Lesions in mammograms include masses, calcifications, and architectural distortions [4-6]. Segmentation is the only available tool for detecting these lesions. Some mammogram information such as breast boundary, tissues, nipple, and pectoral muscle can be used to register

sequence of mammograms. Image registration attempts to map information in a series of images using these landmarks [2-3]. The focus of this paper is to use supervised machine learning algorithm for the detection of these landmarks as inputs for mammogram registration.

A machine learning algorithm classifies input data to its proper class based on previous knowledge learned from a training set. This is done by determining the boundaries or margins that best separate the classes. Decision boundaries are defined using the points that are close to the margins. In a support vector machine (SVM) algorithm these points are known as support vectors. In this paper, we present a relatively new machine learning algorithm that is known as margin setting algorithm (MSA). MSA uses prototypes to determine the decision boundaries [9-12]. MSA has been applied to applications such as artificial colours segmentation, noise estimation, and hyperspectral [7], [15], [17-18]. Recently, a Fourier-based MSA was proposed to recognize the shape, size, pose, and location of a target in a scene [13]. MSA appears to provide better results for classifying nonlinear patterns compared with other machine learning algorithms such as SVM and neural network (NN) [17-18].

MARGIN SETTING ALGORITHM

Margin setting algorithm (MSA) is considered as a machine-learning algorithm. A machine-learning algorithm consists of two phases: learning and classification. The learning phase uses a set of input patterns with a known class (training dataset). In this phase, features such as length, shape, colour, or intensity values, are extracted from each pattern. Only the features that classify the patterns to their classes are selected. Decision boundary is defined between patterns of different classes. The decision boundaries are used in the classification phase to classify the testing patterns to their corresponding classes. When a machine learning algorithm is designed to segment an object in a gray scale image, the input features may be the intensity values and the output classes are the object and background. MSA creates number of prototypes of normal distribution to compute the decision boundaries.

TRAINING PHASE - PARTITION PROCESS

The partition process starts by subdividing the original training set, S, into number of smaller subsets. This is mainly done to search for a prototype for each subset. The subsets should not overlap and should cover the entire set as given in the following equation:

$$S = \underset{i>1}{U} S_i \tag{1}$$

where S_i is a non-empty subset and $S_i \bigcap S_j = \varnothing$ for $i \neq j$. For each subset, a prototype *G* is generated. *G* has a decision boundary that is identified by a radius and a centre. *G* is defined as:

$$G = \{(\delta_k, r_k, \eta_m),\ 1 \le k \le M,\ 1 \le m \le P\} \tag{2}$$

δ_k and r_k are the center and radius of G, respectively, η_m is the class label with P total number of classes, and M is the number of prototypes that belong to class η_m. In the beginning, *N* random points are selected as initial prototypes. The random prototypes are selected within the same range of the points in the training set using normal distribution. The Euclidean distance between each prototype and the points in the training set is computed. Fig. 1 a) shows a training set of two classes, class and non-class sets, with 10 points for the class set that are shown as red '*' symbol and 10 points for the non-class set that are shown as blue '+' symbol. Four prototypes are shown as cyan 'o' symbol.

TRAINING PHASE - EVOLUTION PROCESS

The evolution process computes the optimal prototypes using the initial ones constructed during the partition process. Prototypes with a minimum distance to a point in the class set and of maximized zero-margin radius are considered as potential prototypes. Zero-margin is defined as the distance from the centre of the prototype to the closest non-class point. In Fig. 1 a), only two prototypes satisfy these conditions and considered as potential prototypes for mutation 0 as seen in Fig. 1 b). The distance between each potential prototype and the closest class point and the zero-margin radius are shown in Fig. 1 b). Figure of merit is defined as the number of points from the class set around a potential prototype that are within the zero-margin radius. Figure of merit is a measurement of true positive rate for a given prototype. Each prototype has its own figure of merit. The figure of merits for the two prototypes given in Fig. 1 b) are enclosed by green and purple hyper-planes and are equal to 3 and 6, respectively. The maximum value for the figure of merit is called the generational characteristic value, MF_{mi}. A potential prototype with MF_{mi} is considered as the best prototype.

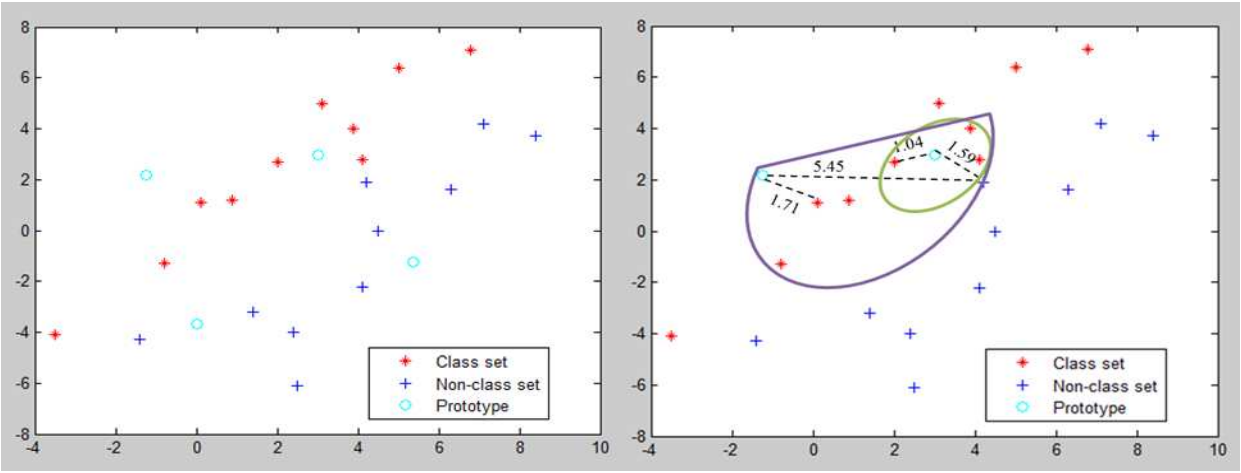

Fig. 1 a) Constructing initial prototypes, and b) potential prototypes with their corresponding figure of merits

If the potential prototypes for the zero mutation do not cover all the points within the class set, then a new mutation is started to compute new prototypes for the unclassified points. The magnitude of the new mutation is computed as:

$$\tau = \varepsilon\alpha\mu \tag{3}$$

where ε is a random sign symbol, $\alpha \in [0,1]$, and μ is the maximum perturbation that is computed as:

$$\mu = \begin{cases} Mx + \delta_k, & \text{if } \delta_k > \dfrac{\text{Mx+Mn}}{2} \\ \delta_k, & \text{otherwise} \end{cases} \tag{4}$$

Mx and *Mn* are the maximum and minimum values in the training set, respectively. The potential prototypes for the new mutation are computed using the equation:

$$N_{n1} = \delta_{k0} + \tau \tag{5}$$

where N_{n1} is the random points for first mutation and δ_{k0} is the centre of a potential prototype in mutation 0 that is chosen as:

$$\sum_{b=1}^{k-1} f_b < \varsigma \leq \sum_{b=1}^{k} f_b \tag{6}$$

ς is a random number $\in [0,1]$ and f_b is the normalized figure of merit computed as:

$$f_m = \frac{F_{mi}}{\sum_{mi=1}^{gm} F_{mi}} \tag{7}$$

gm is the total number of potential prototypes for a given mutation. The mutation process is continued until all points in the class set are trained using a potential prototype or when the maximum number of mutations (*MM*) is reached. There is *MG* number of generations for the training phase and for each generation there is *MM* mutation. The same procedure can be carried out to select prototypes for the non-class set.

Classification Phase

During the classification phase the Euclidean distance between the selected prototypes and all the points in the testing set, $T = \{\gamma_1, \gamma_2, ...,\gamma_i\}$, is computed. γ_i, is a point from the testing set and it is assigned to the class with the smallest Euclidean distance.

MSA for Image Segmentation

Fig. 2 graphs MSA for image segmentation. The steps involved in the algorithm can be summarized as the following:

Step 1, **Construction of the training set:** Select M random points from the test image to construct the training set $t = \{x_i, \text{ for } i = 1 \text{ to } M\}$. t is a 1-D vector with intensity values that are corresponding to both object and background classes.

Step 2, **Construction of initial prototypes:** Create the initial prototypes within the training set intensity range and using normal distribution. The initial prototypes are represented mathematically using Equation (2).

Step 3, Select potential prototypes from initial prototypes: Examine each prototype to select the potential prototypes of minimum Euclidean distance to the object points and of maximized zero-margin radius.

Step 4, Select final prototype for current mutation: Compute the figure of merit for each potential prototype. The prototype with MF_{mi} is selected as the final prototype for a given mutation.

Step 5, **Mutation to N points:** Mutate δ_k of prototype G using Equation (5).

Step 6, **Comparison:** Repeat Steps 2 through 5 until all the training points are trained or when the maximum number of mutations, *MM*, is reached. Based on experimental results, *MM=20* provided good outcome for our dataset.

Step 7, Start new generation: If at least one point in the training set is not classified, then start a new generation and reset the mutation to mutation 0.

Step 8, **Stop condition:** Proceed to the classification step if all the points in the training set are classified or when the maximum generation, *MG*, is reached. Based on experimental results, *MG=20* provided good outcome for our dataset.

Step 9, **Object classification:** Classify each pixel in the image, γ_i, to its corresponding class using the saved prototypes. γ_i is considered as object point if it has minimum Euclidean distance within the zero-margin radius.

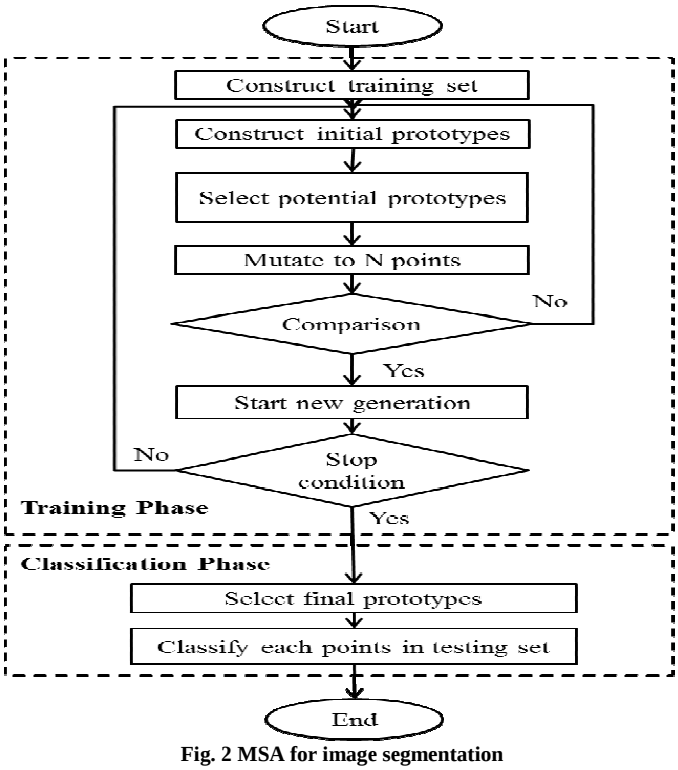

Fig. 2 MSA for image segmentation

RESULTS AND DISCUSSION

Dataset

The segmentation algorithm is implemented on 554 full field digital mammography images for 125 patients. The mammograms are of CC and MLO views. The pectoral muscle segmentation algorithm is implemented on the mammograms with MLO views only, with total number of 284 mammograms. Four mammograms with MLO view have no pectoral muscle and eliminated from pectoral muscle segmentation evaluation step. The dataset is a private one provided by two radiologists who perform screening mammography in USA and Europe. The two radiologists provided the annotation for their datasets. All malignant cases are biopsy proven. Of the cases, 40 were of malignant nature; four cases have lesions of different shapes, seven with masses, eight with calcifications, three with architectural distortions, fourteen with asymmetric densities, and four with asymmetric densities and architectural distortions. The cancer free cases consist of 39 normal cases, three cases with masses, 41 cases with calcifications, one case with architectural distortion, and one case with asymmetric density. The dataset included two cases with implants. The density distribution for the cases is determined using BI-RADS classification. 36 of the cases are almost fatty, 26 are with scattered fibroglandular tissue, 45 are heterogeneously dense, and 18 are extremely dense.

Experimental Results

MSA algorithm is used to separate the breast from the background in the full field digital mammography images. During the training phase of MSA algorithm, the decision boundaries are computed using intensity values. Random points from the object and the background are selected for that purpose. The object is defined as the breast and the rest of the image information is the background. 20 points have been shown as a sufficient number to segment the object regardless of its degree of non-uniformity. As the background is more uniform, fewer points are needed. In the classification phase, the breast is classified using the computed decision boundaries. All the intensity values in the mammogram are the input for the classification phase. A post-processing operation using a median filter of size 5x5 is used to remove impulse noise. MSA performance is subjectively compared with NN and several thresholding algorithms: ACO, global, and Otsu [1], [8], [16], [19]. The input images for each algorithm are DICOM format of raw data and of size approximately 4000x3328. NN algorithm uses the same training and testing data points used for the MSA algorithm. For the thresholding techniques, high intensity values, 15% of the maximum intensity values for each mammogram, are removed to reduce the variation in the gray scale level and increase the accuracy of the segmentation step. A similar approach is applied for the detection of pectoral muscle. Again, the problem involves two classes; the pectoral muscle region and background classes. The background class consists of the rest of the breast region, i.e., parenchymal fatty tissues and the mammogram background.

First, MSA is compared with ACO, global, and Otsu thresholding. The subjective evaluation is done by four experts in the area of pattern recognition using GUI software. One expert is the developer of the algorithm. The other three experts are a Ph.D. and two Ph.D. candidates. The segmented images are positioned randomly in the GUI with no title and are shown side by side on the same page. The order of the segmented images is scrambled so they would not appear at the same position for different cases. The experts compared them with the original mammogram to determine which method provided better results. Table 1 and 2 show the results of subjective evaluation for breast segmentation in MLO and CC views, respectively. Note that when at least two algorithms provided similar results the output was considered to be the same. Fig. 3 shows the results of breast segmentation using the different thresholding techniques and MSA for four different mammograms. MSA performance was superior in comparison to the other thresholding algorithms. As the breast density decreases, it has been noted that Otsu and global thresholding failed to detect the fatty tissues within the parenchyma. When the mammogram has a gradual change in the gray scale level with no sharp edges that separate the background from the skin line, ACO failed to detect the skin line and the fatty region behind it.

Table -1 Subjective Evaluation of Breast Segmentation in MLO View using Four Algorithms

Researcher\Algorithm	ACO	Global	MSA	Otsu	Same
Developer	0	0	268	0	16
Ph.D. Professor	17	6	254	3	4
Ph.D. Candidate 1	6	2	268	2	6
Ph.D. Candidate 2	2	1	273	0	8
Average	6	2	266	1	9

Table -2 Subjective Evaluation of Breast Segmentation in CC View using Four Algorithms

Researcher\Algorithm	ACO	Global	MSA	Otsu	Same
Developer	0	0	257	0	13
Ph.D. Professor	0	0	258	1	11
Average	0	0	257	1	12

Table -3 Subjective Evaluation of Breast Segmentation in MLO View using MSA and NN

Researcher\Algorithm	MSA	NN	Same
Developer	77	15	192
Ph.D. Professor	65	31	188
Ph.D. Candidate 1	140	19	125
Average	94	22	168

Table -4 Subjective Evaluation of Breast Segmentation in CC View using MSA and NN

Researcher\Algorithm	MSA	NN	Same
Developer	133	8	129
Ph.D. Professor	128	31	111
Average	130	20	120

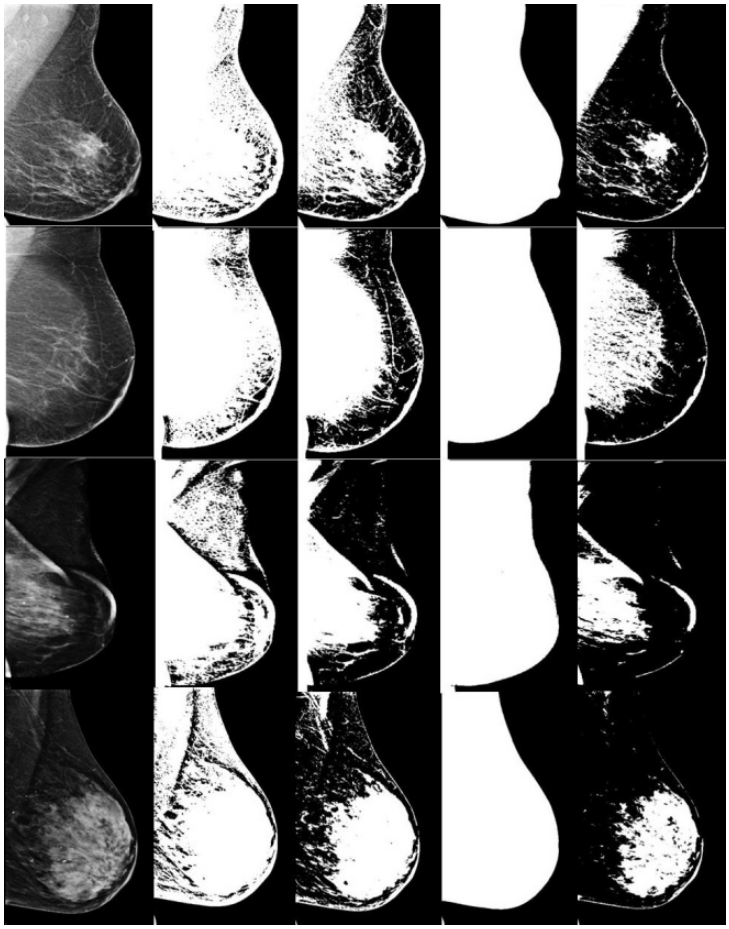

Fig. 3 Breast segmentation, a) original mammogram, b) ACO, c) global, d) MSA, and e) Otsu thresholding, respectively

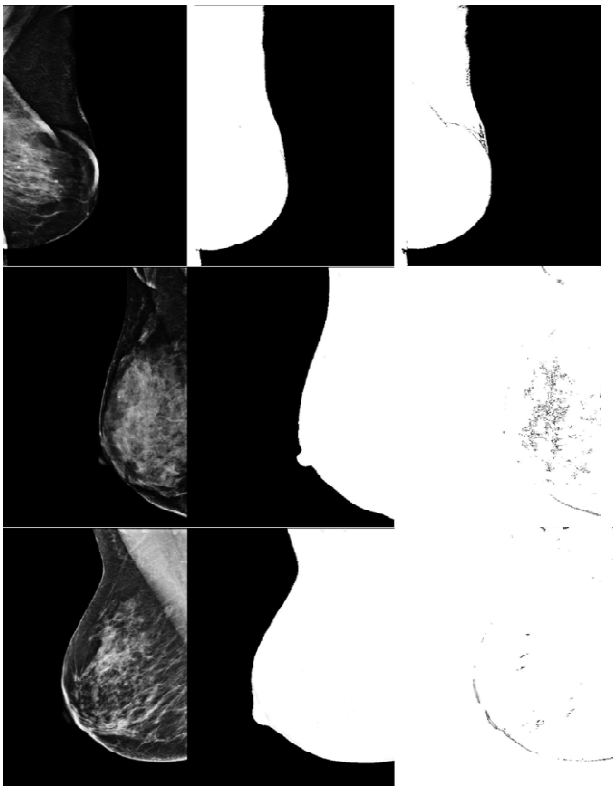

Fig. 4 Breast segmentation in MLO view for three mammogram, a) original mammogram, b) MSA, and c) NN, respectively

To overcome the big difference in performance between MSA and the thresholding techniques, MSA output is compared with NN output. The outputs of the comparison are given Tables 3 and 4 for MLO and CC views, respectively. Fig. 4 displays the segmented breast using MSA and NN algorithms for three mammograms with MLO view. NN detected the breast in most cases but did not provide smooth edges, especially when the breast is not well separable from the background with no visible sharp edge. Also, it did not provide good segmentation for almost fatty breasts. On the other hand, MSA provided better segmentation for the breast regardless of the breast type. Detection of the nipple when it is shown in the profile was also not fully accomplished by NN algorithm. MSA algorithm provided better results in detecting the nipple, even when it is with small intensity values that are close to the background intensity value.

For pectoral muscle segmentation, the segmented images using ACO, global, MSA, and Otsu are subjectively evaluated to determine which algorithm provided a better result in isolating the pectoral muscle from the rest of the mammogram information. A protocol similar to the one used in evaluating the breast segmentation is applied here. The results are given in Table 5. Fig. 5 illustrates the results of the segmented images using ACO, global, MSA, and Otsu, respectively, for four mammograms. The performance of MSA algorithm in detecting the pectoral muscle highly depends on the breast type, i.e., almost fatty, scattered fibroglandular, heterogeneously dense, and extreme dense. When the breast type is almost fatty or fibroglandular tissue, then the parenchymal tissue is completely separable from the pectoral muscle. In this case, MSA provided excellent results. Also, MSA provided good results for heterogeneously dense breasts. The challenge is the extreme dense breast in which the breast mostly consists of fibroglandular tissue and it is not separable from the pectoral muscle. Comparing the performance of the other three algorithms, i.e., ACO, global, and Otsu, in detecting the pectoral muscle illustrated that Otsu provided better segmentation followed by global and then ACO. The three algorithms provided acceptable results for mammograms of scattered fibroglandular and heterogeneously dense breasts. The corresponding mammogram has parencyhmal tissue that is well separable from the pectoral muscle with fatty tissue in the region between the pectoral muscle and parenchymal tissue. However, the three algorithms provided bad detection of pectoral muscle when the breast type is extreme dense or almost fatty. When the breast type is almost fatty, lots of fatty tissues are falsely detected as part of pectoral muscle.

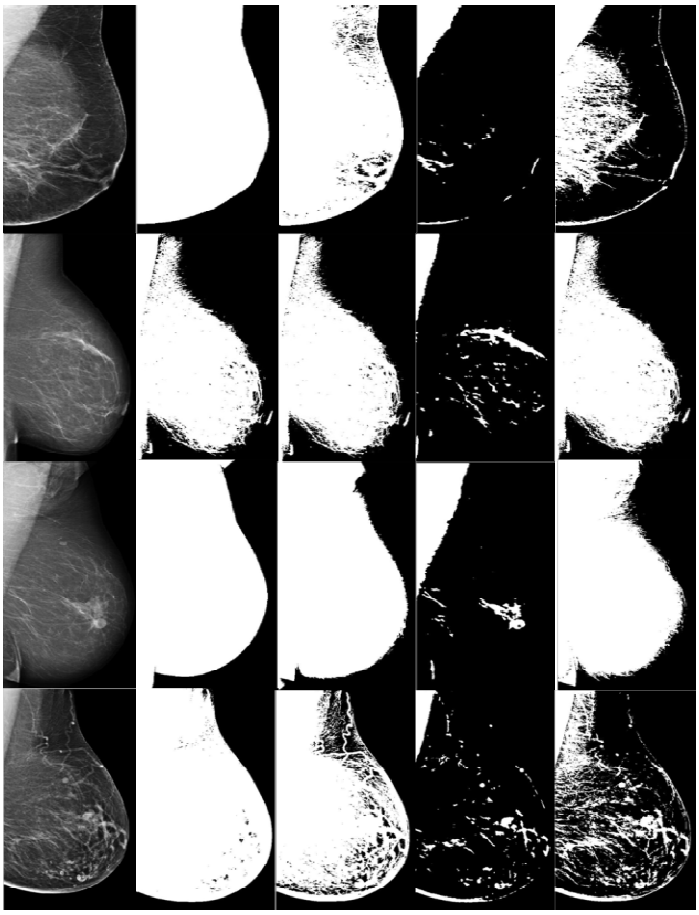

Fig. 5 Separation of pectoral muscle from the rest of breast tissues and background, a) original mammogram, b) ACO, c) global, d) MSA, and e) Otsu thresholding, respectively

Table -5 Subjective Evaluation of Pectoral Muscle Detection in MLO using Four Different Algorithms

Researcher\Algorithm	ACO	Global	MSA	Otsu	Same
Developer	2	5	120	36	117
Ph.D. Professor	4	10	105	44	117
Ph.D. Candidate 1	16	24	155	71	14
Ph.D. Candidate 2	5	5	132	52	86
Average	7	11	128	51	83

MSA for pectoral muscle segmentation is also compared with NN algorithm. The results of subjective evaluation are given in Table 6. NN algorithm provides good segmentation results for almost fatty breast types. However, for scattered fibroglandular breasts, the fibroglandular tissue located next to the pectoral muscle are falsely detected as pectoral muscle as seen in Fig. 6. Also, NN did not provide good detection for extreme dense breast types.

Table -6 Subjective Evaluation Pectoral Muscle Detection in MLO using MSA and NN

Researcher\Algorithm	MSA	NN	Same
Developer	92	55	133
Ph.D. Professor	53	78	149
Average	73	66	141

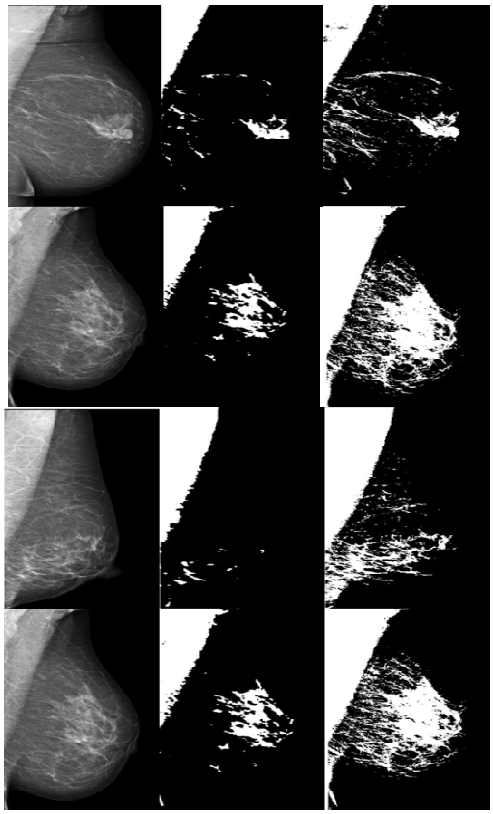

Fig. 6 Pectoral muscle segmentation using MSA and NN

CONCLUSION

A machine learning algorithm to detect the breast and pectoral muscle is presented. This algorithm is known as the margin setting algorithm (MSA). MSA is a relatively new supervised algorithm that utilizes prototypes to determine decision boundaries that best separate nonlinear input patterns. We tested the algorithm on 554 mammograms for MLO and CC views from 125 patients. The algorithm performance has been compared with four algorithms; neural network, ant colony optimization, global, and Otsu thresholding. For the detection of breast, the new algorithm provided better results for 84.21% of the mammograms compared with 15.79% for NN algorithm. For the detection and separation of the pectoral muscle from the rest of the breast tissues, MSA provided better results for 52.52% compared with 47.48% for NN algorithm. Also, MSA accuracy was 64.97% compared with 3.55%, 5.85%, and 25.89% for ACO, global, and Otsu thresholding, respectively.

Acknowledgements
The authors are grateful to Dr. Melanie Scott for her guidance to have better understanding for mammogram analysis and the current challenges in computer-aided diagnosis systems.

REFERENCES

[1] R C Gonzalez and R E Woods, *Digital Image Processing*, 3rd edition, Prentice Hall, **2008.**
[2] A Goshtasby, *2-D and 3-D Image Registration for Medical, Remote Sensing, and Industrial Applications*, John Wiley & Sons, Hoboken, New Jersey, **2005.**
[3] J Hajnal and D Hill, *Medical image registration*, CRC press, **2010**.
[4] L C Hartmann and C L Loprinzi, *The Mayo Clinic Breast Cancer Book*, 1st edition, Good Books, Intercourse, Philadelphia, **2012.**
[5] O J Peart, *Lange Q & A*, McGraw-Hill, New York, **2009.**
[6] L Tabar, T Tot and P Dean, *Understanding the Breast in Health and Disease*, 1st edition, C&C Offset.
[7] J H Caulfield, K Heidary, Exploring Margin Setting for Good Generalization in Multiple Class Discrimination, *Pattern Recognition*, **2005**, vol 38, issue 8, p.1225-1238.
[8] J Tian, W Yu and L Ma, Antshrink, Ant Colony Optimization for Image Shrinkage, *Pattern Recognit Lett*, **2010**, vol. 13, p. 1751-1758.
[9] J Fu, J H Caulfield and A Bandyopadhyay, Pairing Mathematical Morphology with Artificial Color to Extract Targets from Clutter, *Journal of Imaging Sci and Tech*, **2007**, vol. 51, no 2, p.148-154.
[10] J Fu and J H Caufield, Designing Spectral Sensitivity Curves for use with Artificial Color, *Pattern Recognition*, **2007**, vol. 40, issue 8, p. 2251-2260.
[11] J Fu, J H Caulfield, D Wu and W Tadesse, Hyperspectral Image Analysis using Artificial Color, *Journal of Applied Remote Sensing*, **2010**, vol. 4.
[12] J Fu, J H Caulfield, D Wu and T Montgomery, Effects of Hyperellipsoidal Decision Surfaces on Image Segmentation in Artificial Color, *Journal of Electronic Image*, **2010**, vol. 19.
[13] J Fu, J H Caulfield and C Gelnn, Primitive Attempt to Turn Images to Precepts, *International Journal of Machine Learning and Cybernetics*, **2014,** Vol. 5.
[14] H Caulfield, F Jian and Y Seong Moo, Artificial Color Image Logic, *Information Sciences*, **2004**,167,p.1-7.
[15] H Al-Ghaib, R Adhami and H Dinh, An Improved Image Compression Technique Based on Diagonal Edge Estimation, *Proc Of the 5th International Multi-Conference on Engineering and Technological Innovation (IMETI)*, Orlando, Florida,**2012**.
[16] J Fu, H Caulfield and T Mizell, Applying Median Filtering with Artificial Color, *Journal of Imaging Science and Technology*, **2005**, 49(5), 498-504.
[17] Y Wang, R Adhami, and J Fu, A Novel Machine Learning Algorithm for Salt and Pepper Noise Removal, *IEEE Conference, SSP*, **2014.**
[18] H Al-Ghaib and R Adhami, On the Digital Image Additive White Gaussian Noise Estimation, *International Conference on Industrial Automation, Information and Communications Technology (IAICT)*,Bali, Indonesia, **2014**, p.90-96.